Available online at www.sciencedirect.com
ScienceDirect
Journal of Magnetic Resonance 188 (2007) 246–259
JMR Journal of Magnetic Resonance
www.elsevier.com/locate/jmr

Determination of NMR interaction parameters from double rotation NMR

I. Hung [a], A. Wong [a], A.P. Howes [a], T. Anupõld [b], J. Past [b], A. Samoson [b], X. Mo [c], G. Wu [c], M.E. Smith [a], S.P. Brown [a], R. Dupree [a,*]

[a] *Physics Department, University of Warwick, Coventry, CV4 7AL, UK*
[b] *National Institute for Chemical Physics and Biophysics, Akadeemia Tee 23, Tallinn, Estonia*
[c] *Department of Chemistry, Queen's University, Kingston, Canada K7L 3N6*

Received 30 May 2007; revised 18 July 2007
Available online 3 August 2007

Abstract

It is shown that the anisotropic NMR parameters for half-integer quadrupolar nuclei can be determined using double rotation (DOR) NMR at a single magnetic field with comparable accuracy to multi-field static and MAS experiments. The ^{17}O nuclei in isotopically enriched L-alanine and $OPPh_3$ are used as illustrations. The anisotropic NMR parameters are obtained from spectral simulation of the DOR spinning sideband intensities using a computer program written with the GAMMA spin-simulation libraries. Contributions due to the quadrupolar interaction, chemical shift anisotropy, dipolar coupling and J coupling are included in the simulations. In L-alanine the oxygen chemical shift span is 455 ± 20 ppm and 350 ± 20 ppm for the O1 and O2 sites, respectively, and the Euler angles are determined to an accuracy of ± 5–$10°$. For cases where effects due to heteronuclear J and dipolar coupling are observed, it is possible to determine the angle between the internuclear vector and the principal axis of the electric field gradient (EFG). Thus, the orientation of the major components of both the EFG and chemical shift tensors (i.e., V_{33} and δ_{33}) in the molecular frame may be obtained from the relative intensity of the split DOR peaks. For $OPPh_3$ the principal axis of the ^{17}O EFG is found to be close to the O–P bond, and the ^{17}O–^{31}P one-bond J coupling ($^1J_{OP} = 161 \pm 2$ Hz) is determined to a much higher accuracy than previously.

Keywords: Solid-state NMR; Double rotation; Quadrupolar interaction; Chemical shift anisotropy; *J*-coupling; Dipolar coupling; Oxygen-17

1. Introduction

In recent decades, solid-state NMR has developed into an extremely important technique for the characterization of structure and dynamics in condensed matter at an atomic scale. However, the majority of solid-state NMR research has focused on the study of spin $I = 1/2$ nuclei, such as, ^1H, ^{13}C, ^{15}N, etc., rather than nuclei of higher magnetic spin $I > 1/2$, although these nuclei constitute ~75% of the NMR-active nuclei in the Periodic Table. Part of the reason for this is the presence of an electric quadrupole moment for nuclei with spin $I > 1/2$ which interacts with any traversing electric field gradient (EFG), giving rise to the quadrupolar interaction (QI). The QI produces broadening which severely worsens the resolution of resonances. Various techniques have been devised in order to regain high-resolution/isotropic NMR spectra for half-integer quadrupolar nuclei ($I = 3/2$, 5/2, 7/2, 9/2) [1], namely, double angle rotation (DOR) [2,3], dynamic angle spinning (DAS) [2,4], multiple quantum magic angle spinning (MQMAS) [5–7] and satellite transition (ST) MAS [8,9]. The former two techniques require dedicated equipment, whereas the latter two can be achieved using standard (commercial) solid-state NMR equipment. Therefore, since their inception MQMAS and STMAS have seen much greater popularity amongst researchers aiming to obtain isotropic NMR spectra of quadrupolar nuclei.

* Corresponding author. Fax: +44 (0) 24 7652 3412.
E-mail address: R.Dupree@warwick.ac.uk (R. Dupree).

1090-7807/$ - see front matter © 2007 Elsevier Inc. All rights reserved.
doi:10.1016/j.jmr.2007.07.009

Among the techniques mentioned above, only DOR is capable of providing isotropic 1D spectra of quadrupolar nuclei in real time. Rather than relying on sophisticated pulse programming, DOR relies on mechanical sophistication in that the polycrystalline sample is spun simultaneously about two axes subtending the angles 54.74° and 30.56°. This process satisfies the conditions necessary to time-average both first- and second-order perturbations to the Zeeman interaction which have the angular dependences $P_2(\cos\beta) = \frac{1}{2}(3\cos^2\beta - 1)$ and $P_4(\cos\beta) = \frac{1}{8}(35\cos^4\beta - 30\cos^2\beta + 3)$, respectively. Recently, another method for, recording high-resolution 1D spectra in real time using standard MAS probes has been reported. This method (dubbed STARTMAS) is only applicable to $I = 3/2$ nuclei and refocuses the second-order quadrupolar broadening which remains under MAS by correlation of satellite and double quantum transitions [10].

Double rotation (DOR) NMR has seen a gradual development since its original implementation in 1988 [2,3]. In particular, spinning sideband (ssb) suppression [11–15] has been actively pursued, since numerous ssbs are often observed in DOR spectra due to the relatively low limits in outer rotor spinning frequency (currently ~2 kHz). The inherently low sensitivity of NMR has also led to the application of satellite transition saturation/inversion signal enhancement techniques under DOR [16,17]. The majority of DOR NMR studies reported have been concerned with the differentiation of sodium, boron, aluminium and oxygen sites in minerals [18–20], materials [21–25] and molecular sieves, including, zeolites [26–29], sodalites [30–32] and aluminophosphates [33–37]. More recently, focus has turned to exploiting DOR for the study of oxygen sites in organic solids [17,38–41].

Almost all of the DOR NMR literature has concentrated on differentiation, rather than characterization, of quadrupolar nuclei largely due to the predominance of 2D techniques such as MQMAS and STMAS, which serve to provide high-resolution spectra for quadrupolar nuclei using widely available MAS equipment. Hence, few reports have explored the possibility of extracting other NMR interaction parameters from analysis of DOR spectra, particularly chemical shift anisotropy (CSA) [37,42]. The present work aims to examine the usefulness of DOR as a technique complementary to acquisition under MAS and static conditions for the extraction of anisotropic NMR interaction parameters. ^{17}O provides an ideal testing ground for this NMR approach because of the ubiquitous nature of oxygen in a whole range of inorganic [43] and organic [44] materials where oxygen sites play a crucial role in determining properties/behavior and because its NMR spectra often exhibit anisotropic quadrupole and chemical shift effects of comparable strength. Furthermore, the fact that oxygen is a light element means that quantum mechanical calculations of the NMR interaction parameters are feasible which will allow full comparison between experiment and computed values. In the present contribution, [35%-^{17}O]L-alanine (zwitterionic form) and [40%-^{17}O]$OPPh_3$ are used as model compounds to demonstrate the viability of using DOR as a routine tool for the extraction of anisotropic NMR interaction parameters.

2. Theory

Thorough theoretical treatments of NMR interactions and the numerical simulation of their effects can be found in the literature [45–49], including the case where samples are spun about two axes simultaneously, such as for DOR [42,50,51]. As such, the following presents only an overview of the key elements, with particular focus on the QI, for which DOR was developed.

DOR NMR spectra are simulated by density matrix calculation of the expectation value of the spin angular momentum lowering operator, $\hat{I}_-$, yielding a time-domain free induction decay (fid), $s(t)$,

$$s(t) = \left\langle \hat{I}_- \right\rangle = \mathrm{Tr}\{\hat{I}_-\hat{\rho}(t)\}, \tag{1}$$

which is given by the trace of the product between $\hat{I}_-$ and the density matrix as a function of time,

$$\hat{\rho}(t) = \hat{U}(t)\hat{\rho}(0)\hat{U}(t)^{\dagger}. \tag{2}$$

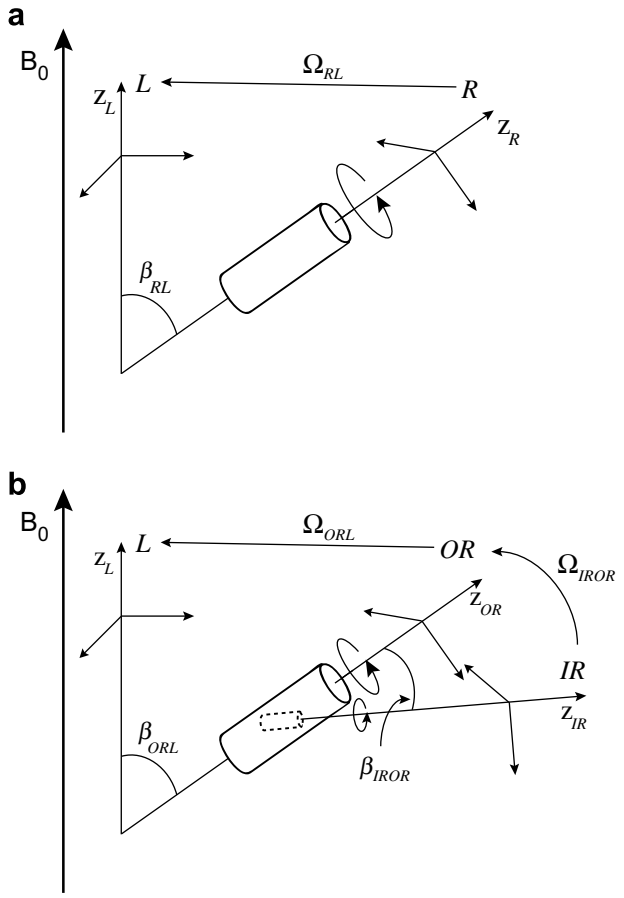

Fig. 1. Schematic depiction of reference frame transformations involved in (a) MAS: rotor (R) → laboratory (L) and (b) DOR: inner rotor (IR) → outer rotor (OR) → laboratory (L).

The propagator, $\widehat{U}(t)$, used to determine the density matrix at time t is calculated from the Hamiltonian operator for the nuclear spin system of concern,

$$\widehat{U}(t) = \exp(-\mathrm{i}\widehat{H}t). \tag{3}$$

According to time-independent perturbation theory, the Hamiltonian can be expressed as the sum of operators for each individual interaction:

$$\widehat{H} = \widehat{H}_Z + \widehat{H}_Q + \widehat{H}_{CS} + \widehat{H}_D + \widehat{H}_J. \tag{4}$$

For a single crystallite orientation, the Hamiltonian operator of each interaction ($\widehat{H}_Z$, Zeeman; $\widehat{H}_Q$, quadrupolar; $\widehat{H}_{CS}$, chemical shift; $\widehat{H}_D$, dipolar and $\widehat{H}_J$, J or scalar) can be expressed in the laboratory frame (L) as a sum of the products of real- and spin-space irreducible spherical tensor operators, A^{λ}_{jm} and $\widehat{T}^{\lambda}_{jm}$, multiplied by a constant C^{λ},

$$\widehat{H}_{\lambda} = C^{\lambda}\sum_{j=0}^{2}\sum_{m=-j}^{+j}(-1)^m[A^{\lambda}_{jm}]^L\widehat{T}^{\lambda}_{j\bar{m}}, \tag{5}$$

where j and m are the rank and order, respectively, of the spherical tensor operators for the interaction λ. L is the coordinate system in which the z-axis coincides with the applied magnetic field.

Determination of the space spherical tensors, $[A^{\lambda}_{jm}]^L$, in the laboratory frame often requires numerous transformations through different reference frames. For example, the transformation from a rotor-fixed frame (R) to L (Fig. 1a) can be described as:

$$[A^{\lambda}_{jm}]^L = \sum_{m'=-j}^{+j}[A^{\lambda}_{jm'}]^R D^j_{m'm}(\Omega_{RL}) \tag{6}$$

where $\Omega_{RL} = (\alpha_{RL}, \beta_{RL}, \gamma_{RL})$ are the Euler angles describing the relative orientation between R and L. The so-called Wigner rotation matrices, $D^j_{m'm}(\Omega_{RL})$, are defined as:

$$D^j_{m'm}(\alpha_{RL}, \beta_{RL}, \gamma_{RL}) = \exp(-\mathrm{i}m'\alpha_{RL})d^j_{m'm}(\beta_{RL}) \times \exp(-\mathrm{i}m\gamma_{RL}), \tag{7}$$

consisting of two exponential terms and a *reduced* Wigner rotation matrix, $d^j_{m'm}(\beta_{RL})$, which can be found tabulated in angular momentum texts (for example, see Ref. [52]).

It can be shown that the Wigner rotation matrix which performs a single transformation can be represented as a composite transformation so that for the case of DOR, $R \rightarrow L$ (Fig. 1a) can be decomposed into inner rotor (IR) $\rightarrow$ outer rotor (OR) $\rightarrow L$ (Fig. 1b),

$$D^j_{m'm}(\Omega_{IRL}) = \sum_{n=-j}^{+j} D^j_{m'n}(\Omega_{IROR})D^j_{nm}(\Omega_{ORL}). \tag{8}$$

Therefore, the transformation sketched in Fig. 1b can be adapted from that of Fig. 1a by modification of Eq. (6) as follows:

$$[A^{\lambda}_{jm}]^L = \sum_{m'=-j}^{+j}\sum_{n=-j}^{+j}[A^{\lambda}_{jm'}]^{IR} D^j_{m'n}(\Omega_{IROR})D^j_{nm}(\Omega_{ORL}). \tag{9}$$

Use of Eq. (7) allows expansion of Eq. (9) into

$$[A^{\lambda}_{jm}]^L = \sum_{m'=-j}^{+j}\sum_{n=-j}^{+j}[A^{\lambda}_{jm'}]^{IR} d^j_{m'n}(\beta_{IROR})d^j_{nm}(\beta_{ORL}) \times \exp\{-\mathrm{i}[m'\alpha_{IROR} + n(\gamma_{IROR} + \alpha_{ORL}) + m\gamma_{ORL}]\}. \tag{10}$$

Due to the spinning of the two rotors under DOR, each of the transformations described in Eq. (9) contains a time-dependent Euler angle corresponding to their respective rotation frequencies, $\alpha_{IROR} = -\omega_{IR}t$ and $\alpha_{ORL} = -\omega_{OR}t$. Therefore, Eq. (10) can be expressed as:

$$[A^{\lambda}_{jm}]^L = \sum_{m'=-j}^{+j}\sum_{n=-j}^{+j}[A^{\lambda}_{jm'}]^{IR} d^j_{m'n}(\beta_{IROR})d^j_{nm}(\beta_{ORL}) \times \exp\{-\mathrm{i}[-m'\omega_{IR}t + n(\gamma_{IROR} - \omega_{OR}t) + m\gamma_{ORL}]\}. \tag{11}$$

β_{IROR} and β_{ORL} are the angles which IR and OR subtend while spinning (i.e., $\beta_{IROR} = 30.56°$ and $\beta_{ORL} = 54.74°$ in the DOR experiment, see Fig. 1b), and γ_{IROR} and γ_{ORL} are the respective phases of IR and OR. In particular, γ_{IROR}

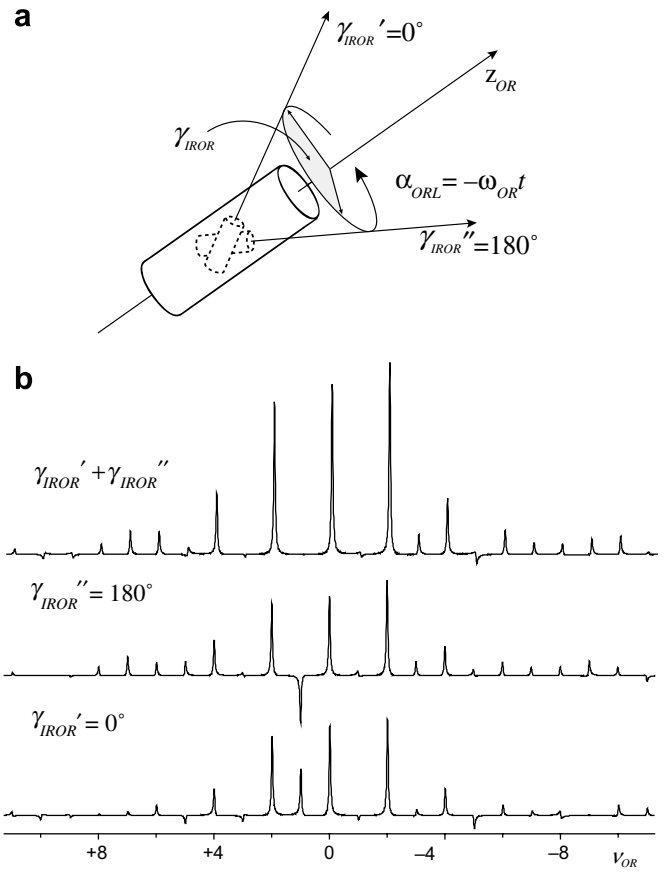

Fig. 2. (a) Schematic depiction of the γ'_{IROR} =0° and γ''_{IROR} =180° outer rotor (OR) positions. (b) Simulated ^{17}O DOR NMR spectra of L-alanine O1 site ($C_Q = 7.86$ MHz, $\eta_Q = 0.28$, $\Omega = 455$ ppm, $\kappa = 0.46$, α_{CE}=38°, $\beta_{CE} = 93°$, $\gamma_{CE} = 98°$) at $B_0 = 14.1$ T illustrating the effect of odd-order spinning sideband suppression.

plays an important role in DOR odd-order spinning sideband suppression (*vide infra*) [11], while γ_{ORL} is analogous to the rotor phase described under MAS [53,54].

The A^{λ}_{jm} terms for each NMR interaction can be expressed most simply in its own principal axis system (PAS). For example, the EFG space spherical tensors in the EFG PAS (E) are given by:

$$[A^{Q}_{00}]^{E} = [A^{Q}_{10}]^{E} = [A^{Q}_{11}]^{E} = [A^{Q}_{1\bar{1}}]^{E} = 0, \tag{12}$$

$$[A^{Q}_{20}]^{E} = 1, \tag{13}$$

$$[A^{Q}_{22}]^{E} = [A^{Q}_{2\bar{2}}]^{E} = -\frac{1}{\sqrt{6}}\eta_{Q}. \tag{14}$$

where $\eta_Q = \frac{V_{11}-V_{22}}{V_{33}}$, $|V_{33}| \geqslant |V_{22}| \geqslant |V_{11}|$ and $\{V_{nn}|n = 1,2,3\}$ are the principal/diagonal components of the EFG tensor in E. For the QI, the constant in Eq. (5) is given by $C^{\lambda} = \frac{1}{\sqrt{6}}\omega_Q$, where

$$\omega_Q = \frac{3C_Q}{2I(2I-1)} \cdot 2\pi, \tag{15}$$

is defined as the quadrupolar frequency (the convention that the satellite transitions appear at $\omega_0 \pm \omega_Q$ is adopted here) and $C_Q = \frac{eQV_{33}}{h}$ is known as the quadrupole coupling constant.

Similarly, the chemical shift (CS) space spherical tensors in the CS PAS (C) are given by:

$$[A^{CS}_{00}]^{C} = -\sqrt{3}\delta_{\text{iso}}, \tag{16}$$

$$[A^{CS}_{10}]^{C} = [A^{CS}_{11}]^{C} = [A^{CS}_{1\bar{1}}]^{C} = 0, \tag{17}$$

$$[A^{CS}_{20}]^{C} = \sqrt{\frac{3}{2}}\delta_{CS}, \tag{18}$$

$$[A^{CS}_{22}]^{C} = [A^{CS}_{2\bar{2}}]^{C} = -\frac{1}{2}\delta_{CS} \cdot \eta_{CS} \tag{19}$$

where $\delta_{\text{iso}} = \frac{1}{3}(\delta_{xx} + \delta_{yy} + \delta_{zz})$, $\delta_{CS} = \delta_{zz} - \delta_{\text{iso}}$ and $\eta_{CS} = \frac{\delta_{yy}-\delta_{xx}}{\delta_{zz}-\delta_{\text{iso}}}$ are defined as the isotropic chemical shift, chemical shift anisotropy (CSA) and CS asymmetry. The $\{\delta_{nn}|n = x,y,z\}$ values are the principal components of the CS tensor defined under the conditions $|\delta_{zz} - \delta_{\text{iso}}| \geqslant |\delta_{xx} - \delta_{\text{iso}}| \geqslant |\delta_{yy} - \delta_{\text{iso}}|$. For the CS interaction, the constant in Eq. (5) is given by the gyromagnetic ratio, $C^{\lambda} = -\gamma$.

The parameters which characterize the CS interaction $(\delta_{\text{iso}}, \delta_{CS}, \eta_{CS})$ are often defined alternatively as the isotropic chemical shift $\delta_{\text{iso}} = \frac{1}{3}(\delta_{11} + \delta_{22} + \delta_{33})$, span $\Omega = \delta_{11} - \delta_{33}$ and skew $\kappa = \frac{3(\delta_{22}-\delta_{\text{iso}})}{\delta_{11}-\delta_{33}}$, where instead the principal components of the CS tensor are defined as $\delta_{11} \geqslant \delta_{22} \geqslant \delta_{33}$ [55].

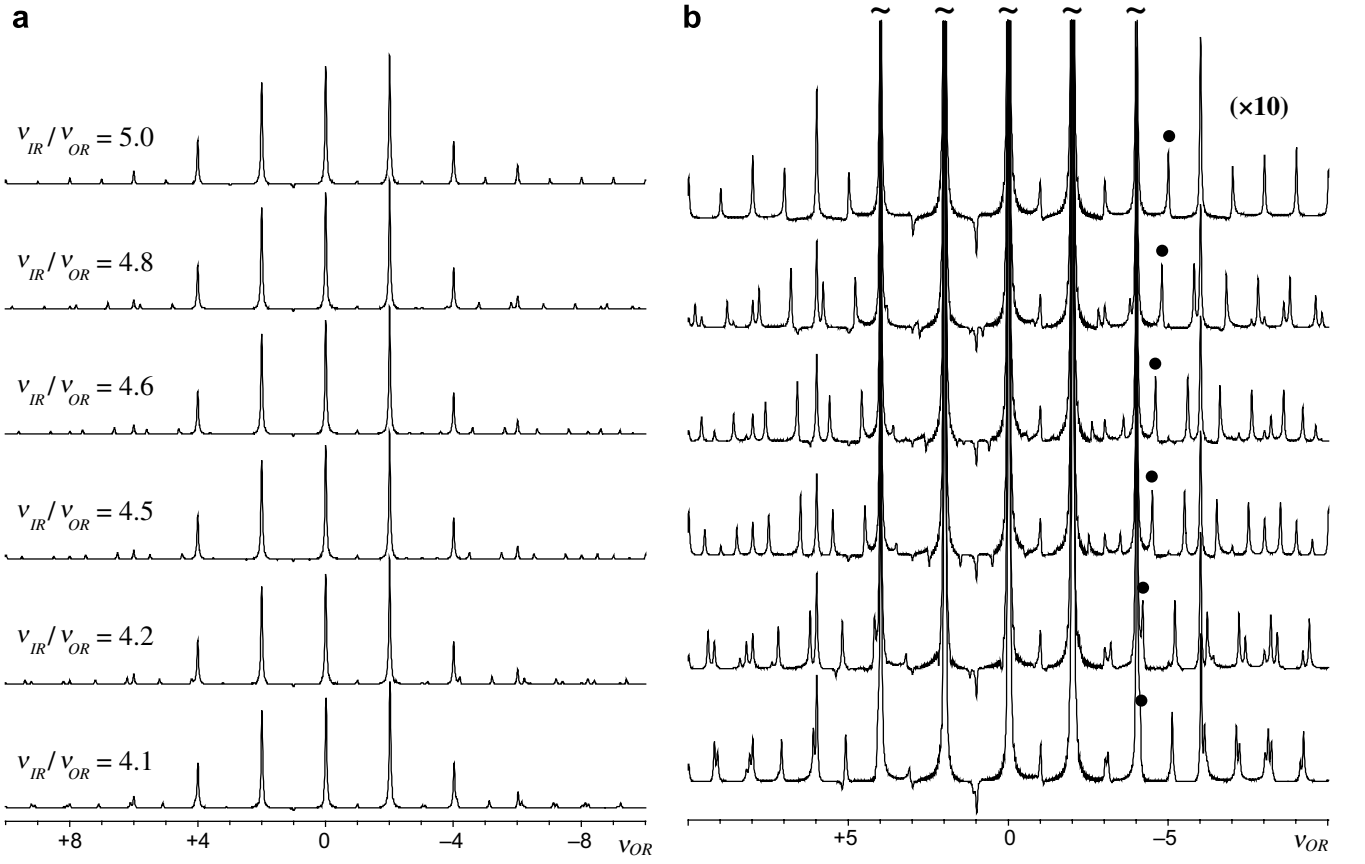

Fig. 3. (a) Simulated ^{17}O DOR NMR spectra of L-alanine O1 site ($C_Q = 7.86$ MHz, $\eta_Q = 0.28$, $\Omega = 455$ ppm, $\kappa = 0.46$, $\alpha_{CE} = 38°$, $\beta_{CE} = 93°$, $\gamma_{CE} = 98°$) at $B_0 = 14.1$ T detailing the effects of changing the *IR* to *OR* spinning frequency ratio, ν_{IR}/ν_{OR}. (b) Vertical expansion of (a) by a factor of 10. Circular markers (●) highlight shifting of the *IR* ssbs as ν_{IR}/ν_{OR} is varied.

Span and skew are used herein since they allow the effects of systematic changes in the CSA to be more readily observed as there is no discontinuity when the middle component passes through the average of the outer components.

The heteronuclear dipolar interaction between two nuclei I and S can be described in its own PAS via the space spherical tensor,

$$[A^D_{20}]^D = \sqrt{6} b_{IS}, \tag{20}$$

where all other $[A^D_{ii}]^D$ are zero, $C^\lambda = 1$, $b_{IS} = -\frac{\mu_0 \gamma_I \gamma_S \hbar}{4\pi \cdot r^3_{IS}}$ is the dipolar coupling constant, r_{IS} is the distance between spins I and S, and γ_I and γ_S are the respective gyromagnetic ratios of I and S.

The underlying assumption of perturbation theory is that most interactions are considerably weaker than the Zeeman interaction. Therefore, in most circumstances it is sufficient to treat NMR interactions as first-order perturbations, such that Eq. (5) simplifies to:

$$\widehat{H}_\lambda = C^\lambda [A^\lambda_{20}]^L \widehat{T}^\lambda_{20}. \tag{21}$$

However, the QI magnitude is often sufficiently large that the perturbation approximation must be extended to second-order. The QI Hamiltonian is then given by:

$$\widehat{H}_Q = \widehat{H}^{(1)}_Q + \widehat{H}^{(2)}_Q \tag{22}$$

where

$$\widehat{H}^{(1)}_Q = \frac{1}{\sqrt{6}} \omega_Q [A^Q_{20}]^L T_{20}, \tag{23}$$

$$\widehat{H}^{(2)}_Q = \frac{\omega^2_Q}{6\omega_0} \left\{ [A^Q_{21}]^L [A^Q_{2\bar{1}}]^L (\widehat{T}^Q_{21} \widehat{T}^Q_{21} - \widehat{T}^Q_{21} \widehat{T}^Q_{2\bar{1}}) + \frac{1}{2} [A^Q_{22}]^L [A^Q_{2\bar{2}}]^L (\widehat{T}^Q_{22} \widehat{T}^Q_{22} - \widehat{T}^Q_{22} \widehat{T}^Q_{2\bar{2}}) \right\}, \tag{24}$$

which result in the nuclear spin energy states

$$E^{(1)}_{Q,m_I} = \frac{1}{6} \omega_Q [A^Q_{20}]^L [3m^2_I - I(I+1)], \tag{25}$$

$$E^{(2)}_{Q,m_I} = \frac{\omega^2_Q}{6\omega_0} \left\{ \begin{array}{l} [A^Q_{21}]^L [A^Q_{2\bar{1}}]^L (4m^3_I - 2m_I I^2 - m_I I + \frac{1}{2} m_I) \\ + \frac{1}{2} [A^Q_{22}]^L [A^Q_{2\bar{2}}]^L (2m^3_I - 2m_I I^2 - 2m_I I + m_I) \end{array} \right\}, \tag{26}$$

where I and m_I are the spin angular momentum quantum numbers, and ω_0 is the Larmor frequency. In the case where more than one perturbing anisotropic NMR interaction is present, all interactions are conventionally transformed from their respective PASs into a molecule-fixed frame (M) and then into the subsequent frames (e.g., IR, OR and L frames) as necessary. In the following, to avoid introducing another frame, M is made equivalent to E.

As is usually the case in solid-state NMR, the case of polycrystalline samples is considered here, such that it is

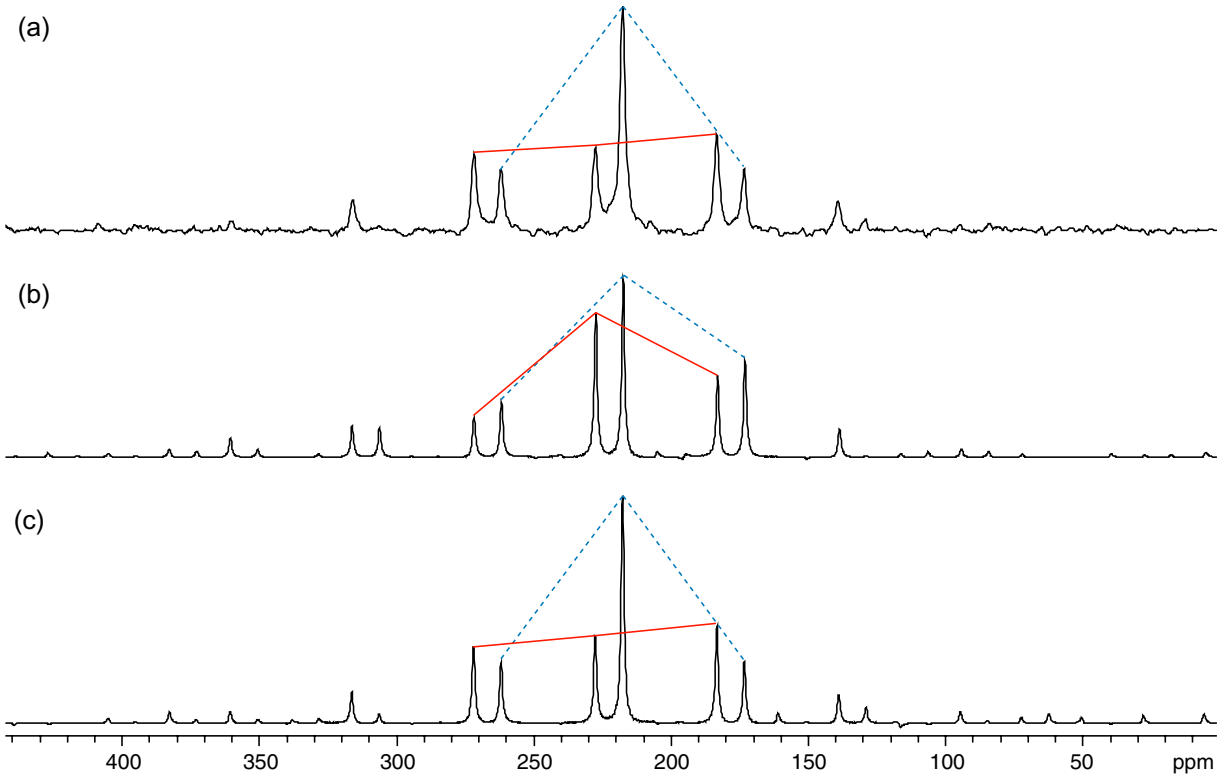

Fig. 4. (a) ^{17}O DOR NMR spectrum of L-alanine (in zwitterionic form), recorded with ^{1}H continuous-wave decoupling (at ~30 kHz ^{1}H nutation frequency) and ssb suppression at $\nu_{OR} = 1805$ Hz and $B_0 = 14.1$ T. 2000 transients were co-added with a recycle delay of 1.0 s, corresponding to an experimental time of ca. 30 min. (b, c) Corresponding simulated spectra using the best-fit parameters (see discussion of Table 1) (b) excluding and (c) including the oxygen CSA.

necessary to average over all possible values of the Euler angles relating E and IR $(\alpha_{EIR}, \beta_{EIR}, \gamma_{EIR})$,

$$\bar{s}(t) = \frac{1}{8\pi^2}\int_0^{2\pi} d\alpha_{EIR}\int_0^{\pi} d\beta_{EIR}\sin\beta_{EIR} \times \int_0^{2\pi} d\gamma_{EIR} s(t;\alpha_{EIR},\beta_{EIR},\gamma_{EIR}), \quad (27)$$

so as to obtain a fid representative of the whole powder [47]. Note that it is only necessary to average over either γ_{EIR} or γ_{ORL}, such that γ_{ORL} is redundant in the notation presented here and can be omitted from Eq. (11). (Note that a powder average over γ_{ORL} with γ_{EIR} redundant is equivalent.)

3. Experimental details

The ^{17}O isotopic enrichment of [35%-^{17}O]L-alanine($^{+}NH_3CH_2CO^{*}O^{*-}$) was carried out using methods

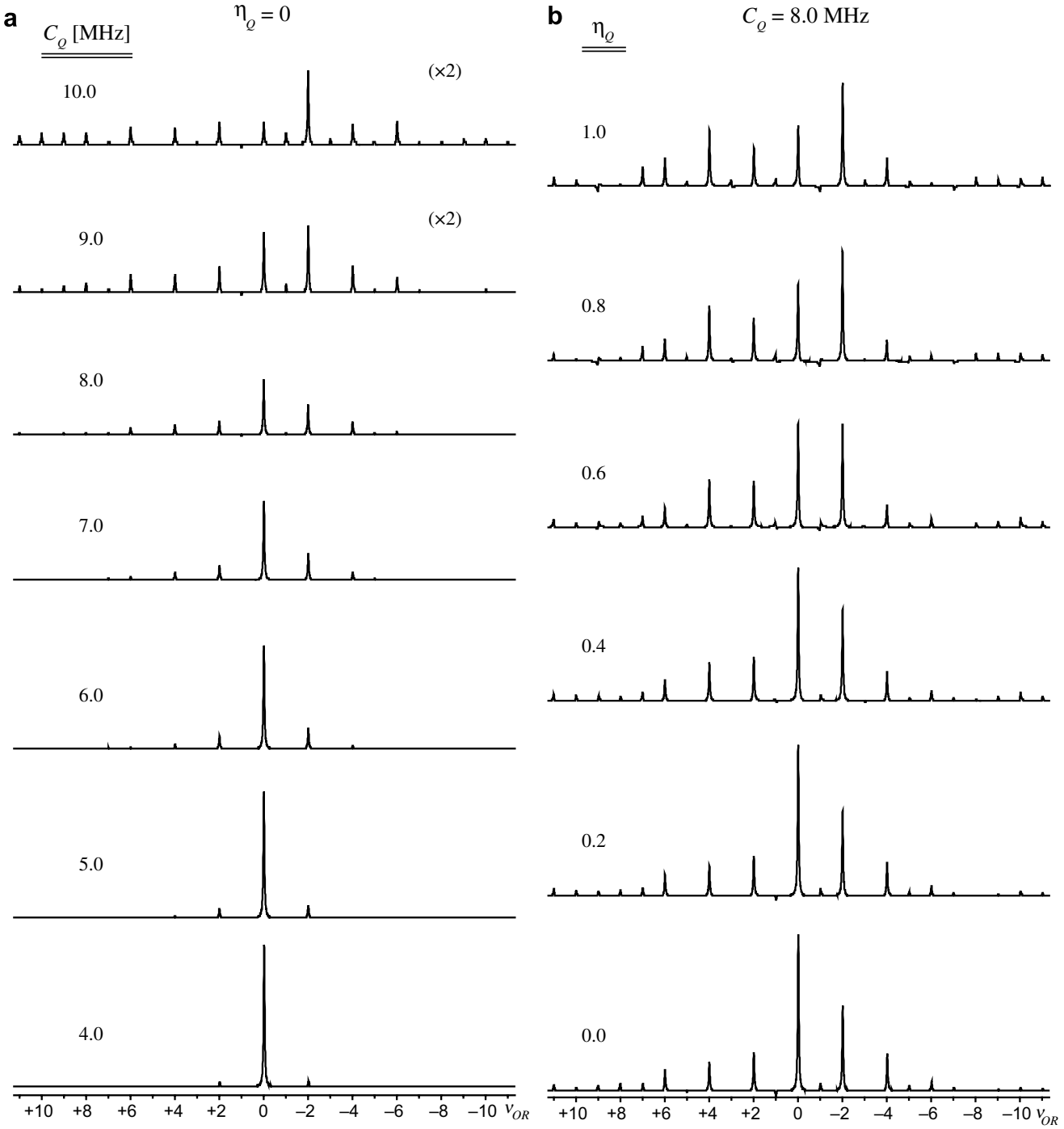

Fig. 5. Simulated ^{17}O DOR NMR spectra at $B_0 = 14.1$ T and $\nu_{OR} = 1805$ Hz (with ssb suppression) showing the effects of varying (a) C_Q with fixed $\eta_Q = 0.0$ and (b) η_Q with fixed $C_Q = 8.0$ MHz. CSA is neglected.

described before [39]. Triphenylphosphine oxide ($OPPh_3$) ($Ph = C_6H_5$) was labelled with [40%-^{17}O]H_2O following the reported method [56] and was recrystallized from acetone to produce the monoclinic polymorph [57].

DOR NMR spectra were acquired on a Chemagnetics Infinity spectrometer at an applied magnetic field of $B_0 = 14.1$ T ($\nu_0(^1H) = 600.1$ MHz) operating at $\nu_0(^{17}O) = 81.3$ MHz. Typical 'central-transition' selective, i.e., scaled by $(I + 1/2)^{-1}$, $\pi/2$ pulses of 4.5 μs at rf fields of 18.5 kHz were employed along with a recycle delay of 1.0 s and continuous-wave ^{1}H decoupling of ~30 kHz. The chemical shift reference for all experiments was H_2O with $\delta_{iso}(^{17}O = 0.0$ *ppm. Unless otherwise stated, experiments were acquired with an outer rotor spinning frequency of* $\nu_{OR} = 1805 \pm 5$ Hz (inner rotor frequency of $\nu_{IR} \sim 7940$ Hz) stabilized by computer control, with odd-order spinning sideband (ssb) suppression (henceforth simply denoted as 'ssb suppression') being achieved by synchronization of the excitation pulse to the outer rotor spinning frequency as described in Ref. [11]. Specifically, the start of acquisition for sequential fids is alternately synchronised to the *OR* positions characterized by $\gamma_{IROR} = 0°$ and $\gamma_{IROR} = 180°$ (Fig. 2a), while each phase cycle step is kept fixed for two acquisitions rather than one.

4. Density-matrix simulation of DOR NMR spectra

Numerical density-matrix simulations of ^{17}O DOR NMR spectra were performed in the time-domain using a program written in C++ and the GAMMA spin-simulation libraries [58]. Unless otherwise stated, simulations were performed with ssb suppression at $B_0 = 14.1$ T, $\nu_{OR} = 1805$ Hz, $\nu_{IR}/\nu_{OR} = 5$, and apodized by an exponential decay function corresponding to a line broadening of ~100 Hz prior to Fourier transformation. Simulation of each DOR NMR spectrum typically required ca. 0.5–3.0 min on a personal computer with a 2.8 GHz Pentium 4 processor and 1.0 GB of RAM.

Simulated spectra in Fig. 2b illustrate how ssb suppression is achieved by synchronization of the excitation pulse to the outer rotor spinning frequency (see Fig. 2a) [11]. If a spectrum is acquired by synchronizing the start of the fid with the $\gamma'_{IROR} = 0°$ *OR* position (Fig. 2b, lower trace), and then recorded again by synchronizing to the $\gamma''_{IROR} = 180°$ *OR* position (Fig. 2b, middle trace), their sum would yield a spectrum with odd-order ssbs of significantly diminished intensity (Fig. 2b, upper trace).

Under spinning, the Hamiltonian describing the system is time-*dependent* making it necessary to partition the evolution period into small steps wherein the Hamiltonian is treated as being time-independent [49]. For arbitrary ν_{IR}/ν_{OR}, simulations require calculation of sufficient propagators to cover the whole evolution period of the fid. However, for an integer value of ν_{IR}/ν_{OR}, it suffices to calculate the propagators spanning a single *OR* period ($\tau_{OR} = 1/\nu_{OR}$). These propagators are then reused to calculate the evolution of the whole fid, leading to much shorter simulation times. This is the procedure for the simulations presented in the following sections. As shown in Fig. 3a, DOR simulations varying the ν_{IR}/ν_{OR} ratio display minimal variation of the prominent spectral features. At a 10-fold magnification of the vertical scale differences become obvious and the additional *IR* ssbs for non-integer ν_{IR}/ν_{OR} ratios are clearly observed. (Fig. 3b).

5. L-Alanine—the effects of the QI and CSA

An experimental ^{17}O DOR NMR spectrum of [35%-^{17}O]L-alanine (in the zwitterionic form), recorded with ssb suppression is shown in Fig. 4a. The two resonances observed at $\delta_{DOR} = 227$ ppm and 217 ppm correspond to the two oxygen sites (O1 and O2) of the CO_2^- moiety in L-alanine, respectively. Previously reported ^{17}O EFG parameters [59] were employed to simulate a DOR spectrum including only the effects of the QI (Fig. 4b). It is evident that inclusion of only the QI provides an inadequate fit of the experimental spectrum particularly for the high-frequency O1 resonance ($\delta_{DOR} = 227$ ppm). Oxygen CSA must also be considered to obtain good agreement with experiment (*vide infra*) (Fig. 4c).

In the following discussion, the effects of the different EFG and CSA parameters on simulated DOR spectra (obtained with ssb suppression) are considered in turn. Consider first the effect of C_Q and η_Q on DOR spectra (in the absence of CSA). A gradual increase in the number of ssbs is observed with increasing C_Q at $\eta_Q = 0.0$ (Fig. 5a) in analogy to an increase in CSA under MAS. In particular when C_Q reaches ca. 9.0 MHz, much of the signal intensity is distributed into the ssbs and the isotropic resonance is no longer most prominent. A similar effect is observed when η_Q is increased beyond 0.6 for $C_Q = 8.0$ MHz. In the presence of small/null CSA, an analysis of the DOR NMR

Table 1
Best-fit ^{17}O DOR simulation parameters

	L-Alanine O1	L-Alanine O2	$OPPh_3$
C_Q (MHz)	7.86 ± 0.10[a]	6.53 ± 0.10[a]	4.57 ± 0.05[b]
η_Q	0.28 ± 0.10[a]	0.70 ± 0.10[a]	0.1 ± 0.1[b]
δ_{iso} (ppm)	285.0 ± 0.5[a]	262.5 ± 0.5[a]	53.0 ± 0.1
Ω (ppm)	455 ± 20	350 ± 20.0	160 ± 10
κ	0.46 ± 0.15	0.40 ± 0.20	−0.75 ± 0.2
δ_{11} (ppm)	478 ± 14	414 ± 14	153 ± 7
δ_{22} (ppm)	355 ± 20	309 ± 20	13 ± 10
δ_{33} (ppm)	23 ± 14	64 ± 14	−7 ± 7
α_{CE} (°)	38 ± 5	30 ± 10	24 ± 5[c]
β_{CE} (°)	93 ± 5	95 ± 5	4 ± 5[c]
γ_{CE} (°)	98 ± 15	102 ± 5	82 ± 5[c]
$^1J_{OP}$ (Hz)	—	—	161 ± 2
$b_{OP}/2\pi$ (Hz)	—	—	−2100 ± 400[d]
β_{DE} (°)	—	—	−5 ± 10

[a] Parameters from Ref. [59].
[b] Parameters from MAS experiment.
[c] The Euler angles in Ref. [56] can be converted to the convention used in this paper by $(\alpha_{CE}, \beta_{CE}, \gamma_{CE}) = (90° - \alpha, 90° - \beta, 90° - \gamma)$.
[d] Calculated from the O–P distance measured via single-crystal X-ray diffraction [64].

spectrum could serve to extract EFG parameters (C_Q, η_Q) in a similar fashion as performed with MAS spectra.

Consider now the combined effect of CSA and QI. For parameters corresponding to the O1 site in L-alanine (see Table 1), a marked sensitivity to the effects of ^{17}O CSA (Fig. 6a) is observed. As the oxygen CS span (Ω) is increased, the intensity of the centreband diminishes with respect to the ± 2 ssbs, while other peripheral ssbs become more intense. The DOR ssb manifold also exhibits sensitivity to the CS skew (κ) as it is varied from -1 to $+1$ with $\Omega = 500$ ppm (Fig. 6b). Notably when $\kappa \geqslant 0.0$, the ssbs spread over a region of approximately 50 kHz. Considering

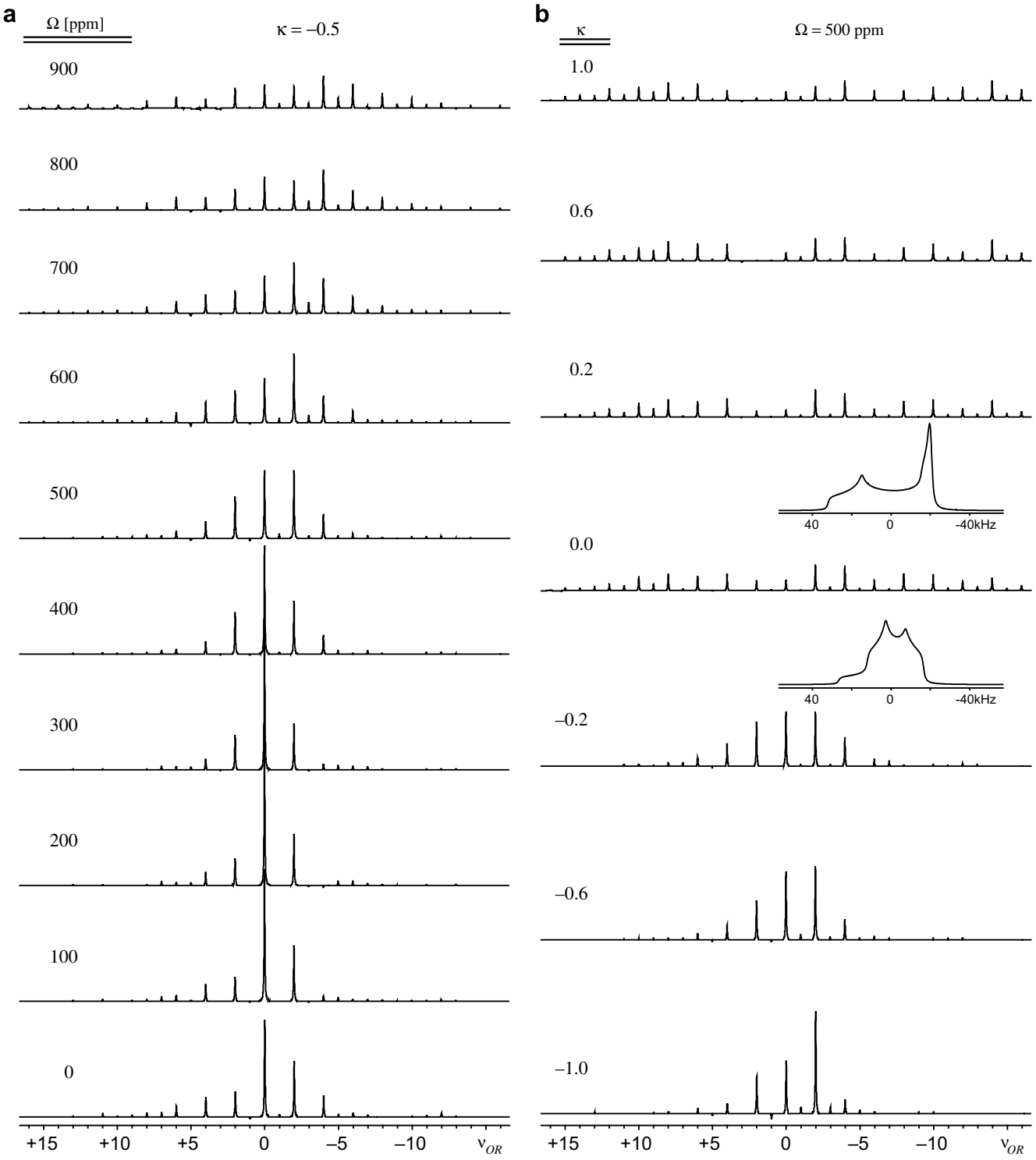

Fig. 6. Simulated ^{17}O DOR NMR spectra at $B_0 = 14.1$ T of the L-alanine O1 resonance ($C_Q = 7.86$ MHz and $\eta_Q = 0.28$) at $\nu_{OR} = 1805$ Hz with ssb suppression and $(\alpha_{CE}, \beta_{CE}, \gamma_{CE}) = (0^\circ, 0^\circ, 0^\circ)$ showing the effects of varying (a) Ω with fixed $\kappa = -0.5$ and (b) κ with fixed $\Omega = 500$ ppm. Insets show static NMR spectra simulated with the same parameters corresponding to the DOR spectra with $\kappa = 0.0$ and -0.2.

that $\Omega = 500$ ppm translates into a breadth of ca. 40 kHz, it is in fact the spectra with $\kappa < 0.0$ that only possess ssb orders up to ± 6 which are intriguing. This is a consequence of the well known fact that the interplay of the EFG and CS tensors has a dramatic effect on the shape and breadth of static NMR powder patterns [56,60,61]; the resulting frequency range is not simply an addition of the effects caused by the individual anisotropic interactions. Hence, it appears that when $\kappa < 0.0$ the effects of CSA are being counteracted by the QI, whereas in the case of $\kappa \geqslant 0.0$ the QI seems to add to the frequency spread caused by the CSA. This is illustrated by insets for $\kappa = -0.2$ and 0.0 showing simulated static spectra: whilst for $\kappa = -0.2$ the major part of the static spectrum is $\sim$30 kHz wide, for $\kappa = 0.0$ the static spectrum covers a frequency range of $\sim$55 kHz.

Further evidence of the interplay of these effects is evident in simulations of DOR spectra varying the relative orientation of the EFG and CS tensors (see Fig. 7). The relative orientation of the ^{17}O EFG and CS tensors is given by the three Euler angles $(\alpha_{CE}, \beta_{CE}, \gamma_{CE})$ that describe the transformation which brings the CS PAS into coincidence with the EFG PAS. Simulated ^{17}O DOR NMR spectra corresponding to the O1 resonance ($C_Q = 7.86$ MHz, $\eta_Q = 0.28$, $\Omega = 455$ ppm, $\kappa = 0.46$) are observed to be very sensitive to variation of $(\alpha_{CE}, \beta_{CE}, \gamma_{CE})$ in both overall shape as well as in the total number of constituent ssbs (Fig. 7), e.g., contrast spectra with $(\alpha_{CE}, \beta_{CE}, \gamma_{CE}) = (45°, 45°, 0°)$ and (0°, 45°, 45°). This indicates that acquisition of DOR spectra represents a useful alternate/additional tool to multi-field static/MAS NMR spectra for the determination of CS/EFG relative orientations. For the O1 resonance, best fit to the experimental spectrum (see Fig. 4c) is found for $(\alpha_{CE}, \beta_{CE}, \gamma_{CE} = (48°, 93°, 98°)$ corresponding to approximately the case of (45°, 90°, 90°) in the bottom middle simulated spectrum in Fig. 7.

The determination of CS parameters for a given site from DOR spectra depends heavily on accurate knowledge of the EFG parameters. It is generally assumed that MAS NMR spectra of quadrupolar nuclei are devoid of CSA effects, allowing extraction of accurate EFG parameters. However, this is not always the case and Fig. 8 presents simulations of MAS (18.05 kHz) powder spectra (performed using SIMPSON [45]) for different magnitudes of Ω at $B_0 = 14.1$ T. The EFG and CS skew are those deter-

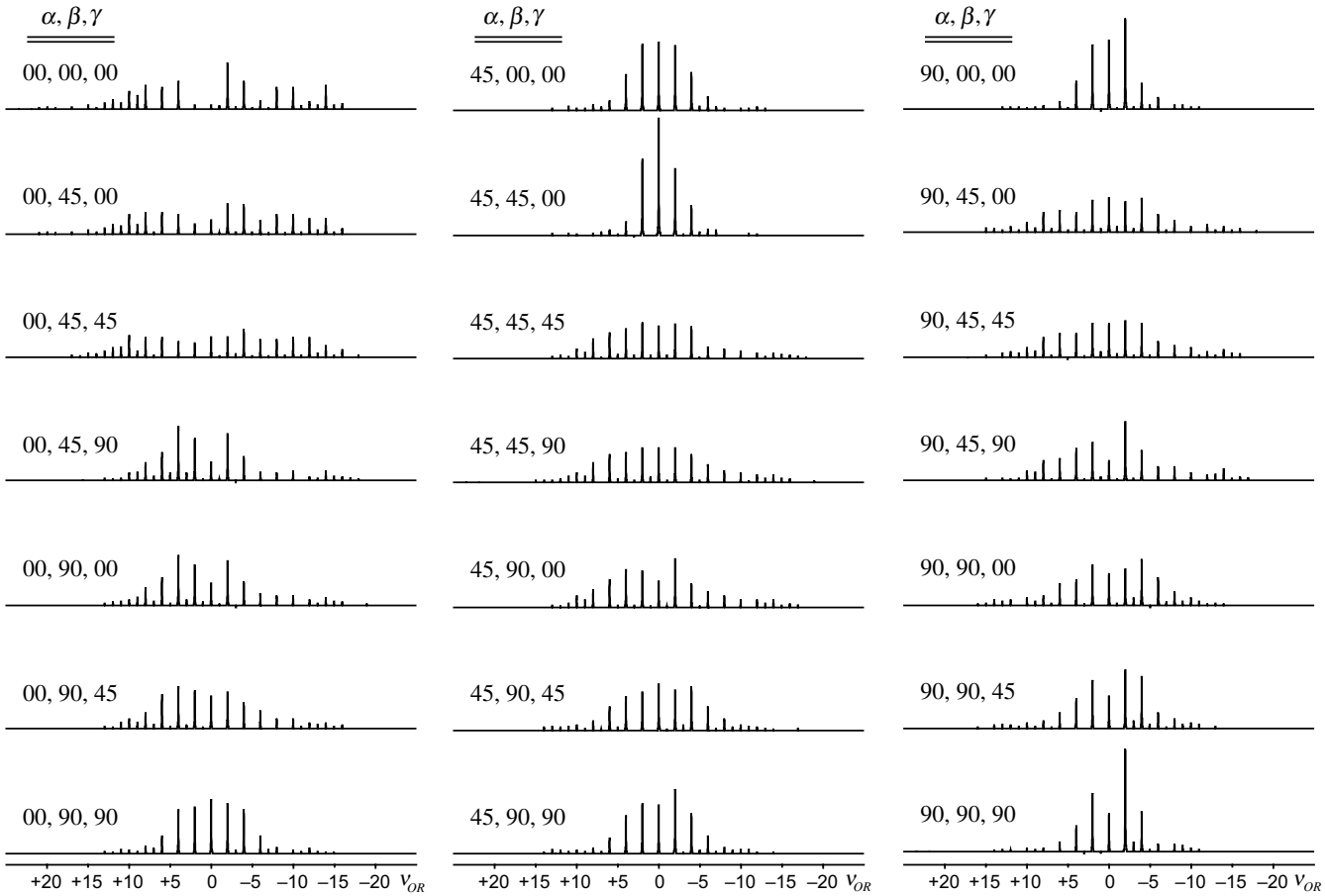

Fig. 7. Simulated ^{17}O DOR NMR spectra at $B_0 = 14.1$ T of the L-alanine O1 resonance ($C_Q = 7.86$ MHz, $\eta_Q = 0.28$, $\Omega = 455$ ppm, $\kappa = 0.46$) at $\nu_{OR} = 1805$ Hz with ssb suppression showing the effects of varying the Euler angles $(\alpha_{CE}, \beta_{CE}, \gamma_{CE})$ describing the relative orientation of the CS and EFG tensors.

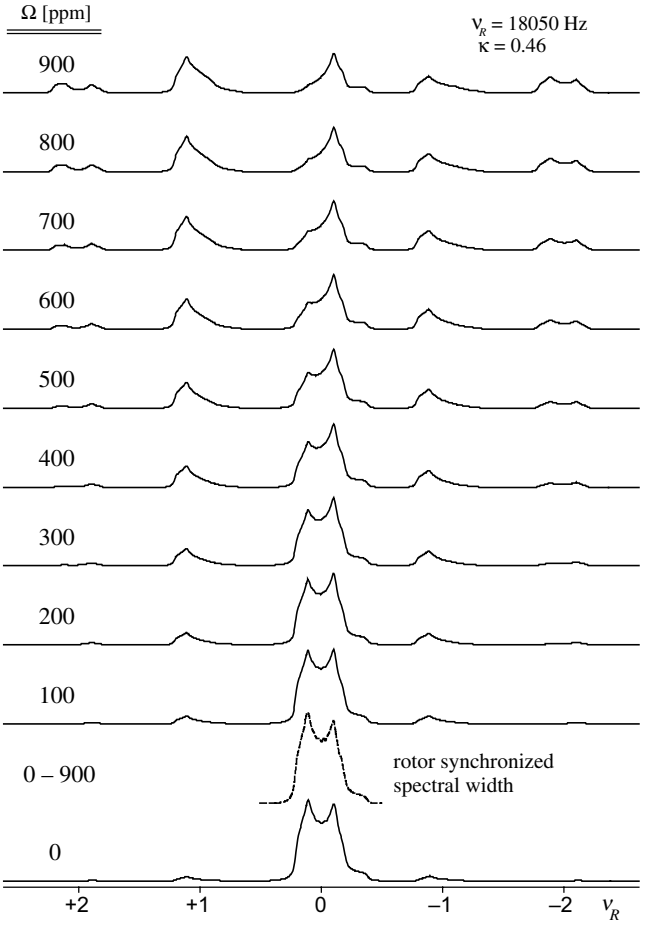

Fig. 8. Simulated (using SIMPSON) ^{17}O MAS NMR spectra at $B_0 = 14.1$ T and $\nu_R = 18050$ Hz showing the effects of increasing CS span (Ω) for EFG and skew corresponding to the L-alanine O1 resonance ($C_Q = 7.86$ MHz, $\eta_Q = 0.28$, κ=0.46) and $\alpha_{CE} = 0°$, $\beta_{CE} = 0°$, $\gamma_{CE} = 0°$. The inset shows that rotor-synchronized MAS spectra (spectral width = MAS frequency) are independent of CSA.

mined from the fit of DOR ssbs for the O1 site in L-alanine (see Table 1), but Euler angles of ($\alpha_{CE} = \beta_{CE} = \gamma_{CE} = 0°$) were used as effects on the MAS spectrum are more noticeable. While the positions of the singularities (upon which spectral fits are based on) in the centreband are independent of the CSA, the shape of the centreband changes considerably as more of the signal intensity is distributed into the ssbs at larger Ω values. Note that at $\Omega \geqslant 600$ ppm, the high-frequency discontinuity declines to such an extent that the incorrect conclusion of the pattern arising from a high asymmetry EFG (i.e., η_Q close to 1.0) could be drawn. Importantly, the rotor-synchronised (spectral width = MAS frequency) MAS spectrum is independent of the CSA parameters, (Fig. 8, inset), i.e., the EFG parameters (C_Q and η_Q) could be determined from rotor-synchronised MAS spectra. An alternative solution to this difficulty would be to refocus more of the signal intensity into the centreband using higher MAS frequencies, which will not always be possible. While, in principle, the CS parameters can be determined from a fit to the centreband and sideband lineshapes, a high signal-to-noise ratio would be required for the low-intensity outer sidebands, and an analysis would be very difficult in the case of multiple overlapping sites.

Table 1 presents the best fit CS parameters for the O1 and O2 L-alanine resonances as determined from a fit of the ^{17}O DOR spectrum in Fig. 4a. The accuracy for the fits is estimated to be ±20 ppm for Ω and ±5°–15° for the Euler angles. For comparison, Table 1 also lists the principal components of the CS tensor (see Section 2). The ^{17}O δ_{iso}, C_Q and η_Q were kept as fixed parameters since they have been determined to a good degree of accuracy from MAS NMR spectra at multiple external magnetic fields [39].

Table 2 compares the ^{17}O NMR parameters for L-alanine as obtained by using the DOR ssbs intensities in the present work with those determined by Yamada et al. from a very recent ^{17}O static, MAS and MQMAS study at multiple external magnetic fields [62]. (Note that we only became aware of the study by Yamada et al. after carrying out the analysis of our ^{17}O DOR data.) The ^{17}O CSA parameters agree very well to within the stated accuracy of the two studies. In particular, all three Euler angles agree to within 3° for O1 and 7° for O2 (once all values are converted into the same convention). The only discrepancy between the two sets of data appears to be in the values of δ_{iso} and/or $P_Q = C_Q\sqrt{1+\eta_Q^2/3}$. The observed ^{17}O DOR NMR shift $\delta_{DOR} = \delta_{iso} - \frac{3}{500}\frac{C_Q^2}{\nu_0^2}(1+\frac{\eta_Q^2}{3})\cdot 10^6$ ppm calculated at $B_0 = 14.1$ T from the (δ_{iso}, P_Q) values of Yamada et al. are 230.4 and 219.8 ppm, which contrast with the values of 227.3 and 217.4 ppm observed for the O1 and O2 sites, respectively. The difference of 3.1 ppm and 2.4 ppm from the experimentally observed δ_{DOR} values is greater than the reported error of ±1 ppm for δ_{iso} or that arising from P_Q. Thus, the error estimates reported in [62] for δ_{iso} and/or P_Q seem to be slightly optimistic.

It is interesting to compare the eight NMR parameters obtained here for L-alanine with recent DFT calculations (also shown in Table 2). The calculation of Gervais et al. [59] was performed under periodic boundary conditions employing the full crystal structure, whereas that of Yamada et al. [62] considered a cluster of molecules. Gervais et al. have compared the values of δ_{iso}, C_Q and η_Q with experiment and found that the calculated values are very sensitive to the structure (the values shown in Table 2 were calculated using the crystal structure refined from neutron diffraction experiments). The Euler angles from both reported calculations agree well with experimental values derived in the present work. However, although κ is in reasonable agreement with experiment, the calculated Ω is about 10% too large principally because δ_{11} is approximately 35 ppm larger than the value found experimentally. Such an overestimation of Ω is consistent with other DFT calculations of CSA [63].

Table 2
Comparison of anisotropic ^{17}O NMR parameters extracted for L-alanine

	L-Alanine O1				L-Alanine O2			
	Experimental		Calculation		Experimental		Calculation	
	This work	Ref. [62]	Ref. [59]	Ref. [62]	This work	Ref. [62]	Ref. [59]	Ref. [62]
C_Q (MHz)	7.86[a]	7.80	8.20	8.62	6.53[a]	6.70	6.90	6.97
η_Q	0.28[a]	0.28	0.29	0.23	0.70[a]	0.69	0.67	0.68
δ_{iso} (ppm)	285.0 ± 0.5[a]	287 ± 1	293	312	262.5 ± 0.5[a]	267 ± 1	274	287
Ω (ppm)	455 ± 20	443 ± 10	505	490	350 ± 20	342 ± 10	389	362
κ	0.46 ± 0.15	0.39 ± 0.05	0.44	0.39	0.40 ± 0.20	0.25 ± 0.05	0.30	0.21
δ_{11} (ppm)	478 ± 14	480	508	526	414 ± 14	424	449	455
δ_{22} (ppm)	355 ± 20	344	368	375	309 ± 20	295	314	312
δ_{33} (ppm)	23 ± 14	37	3.0	36	64 ± 14	82	60	93
α_{CE} (°)	38 ± 5	38 ± 4[b]	40	37[b]	30 ± 10	35 ± 4[b]	−30[a]	29[b]
β_{CE} (°)	93 ± 5	90 ± 4[b]	−90	91[b]	95 ± 5	93 ± 4[b]	−95[a]	88[b]
γ_{CE} (°)	98 ± 15	95 ± 4[b]	95	97[b]	102 ± 5	95 ± 4[b]	−95[a]	94[b]

[a] Parameters from Ref. [59]. Note that a change in sign of all 3 Euler angles gives equivalent result.
[b] The Euler angles in Ref. [62] have been converted to the convention used in this paper by using $(\alpha_{CE}, \beta_{CE}, \gamma_{CE}) = (180° - \gamma, \beta, 90° - \alpha)$.

6. $OPPh_3$—the effects of the QI, CSA, and heteronuclear *J* and dipolar interactions

In [40%-^{17}O]$OPPh_3$, one-bond ^{17}O–^{31}P *J* coupling ($^1J_{OP}$) leads to a splitting of both the centreband and ssbs, which is shown in the slow spinning ^{17}O DOR spectrum *without* ssb suppression (Fig. 9a). A relatively low *OR* spinning rate ($\nu_{OR} = 900$ Hz) was employed so that the effects of the smaller QI and CSA for this sample (relative to L-alanine) can be observed in the ssb intensities. As with L-alanine, line narrowing was achieved using ^1H decoupling. Even for the weak O···H interactions in $OPPh_3$, where the shortest O–H distances are ca. 2.5 Å [64], the linewidth of each peak in the DOR centreband narrowed from 136 to 80 Hz when a ^1H decoupling field of approximately 28 kHz was used during acquisition. Owing to the high spectral resolution achieved via DOR, a splitting of the isotropic resonance due to $^1J_{OP}$ can be clearly observed and readily determined to high accuracy (~1%). The observed $^1J_{OP}$ (161 ± 2 Hz) agrees well with values measured in the ^{17}O MAS NMR spectrum (150 ± 20 Hz) [56] and in $CDCl_3$ solution (160.0 ± 2.4 Hz) [57].

There is a difference in the relative intensities of the two components of the line (observable in both the centreband and ssbs) which can only be accounted for by inclusion of the ^{17}O–^{31}P dipolar interaction. In the cases where only the combination of interactions $J + QI$ (Fig. 9b) or $J + QI + CSA$ (Fig. 9c) are included, the two components have the same relative intensities in the centreband and ssbs. Whilst the effect of including the dipolar coupling and neglecting CSA changes their relative intensity (Fig. 9d), only by including all interactions is it possible to obtain agreement with the experimental spectrum (Fig. 9e). Simulations demonstrate that the relative intensities of the two peaks in the centreband are very sensitive to Ω (Fig. 10a). For small Ω, the low-frequency peak is significantly smaller than the high-frequency peak, however when $\Omega = 120$ ppm their relative intensities are reversed. The ssbs initially decrease in intensity as Ω increases but begin to increase significantly for $\Omega > 100$ ppm. The relative intensities of the two centreband components are much

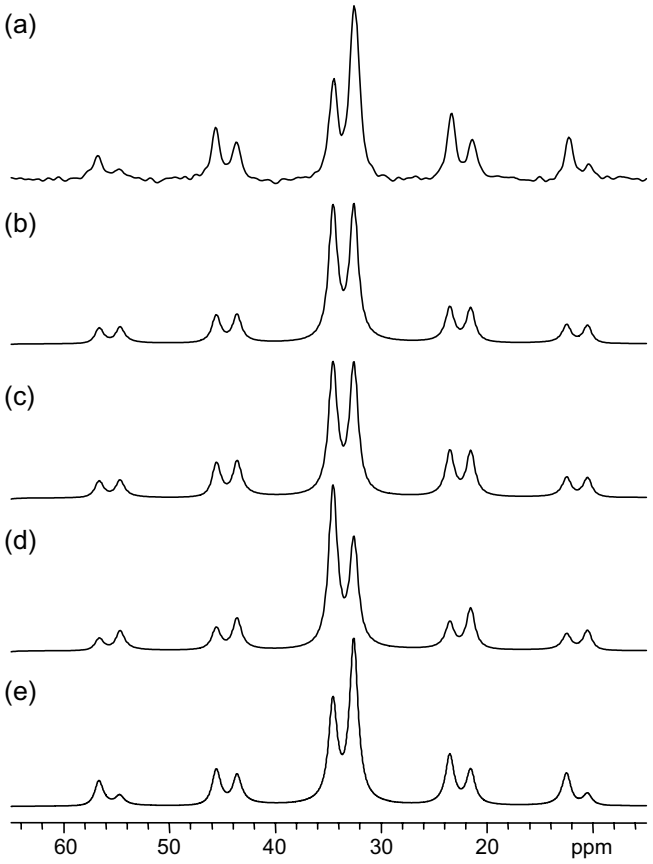

Fig. 9. ^{17}O DOR NMR spectra *without* ssb suppression of $OPPh_3$ at $B_0 = 14.1$ T, $\nu_{OR} = 900$ Hz, $\nu_{IR}/\nu_{OR} \sim 4.7$, and ^1H continuous-wave decoupling (~28 kHz ^1H nutation frequency): (a) experimental (7516 transients were co-added with a recycle delay of 10.0 s, corresponding to an experimental time ~20 h); simulations including NMR interactions (see Table 1) (b) $J + QI$, (c) $J + QI + CSA$, (d) $J + QI + D$ and (e) $J + QI + CSA + D$.

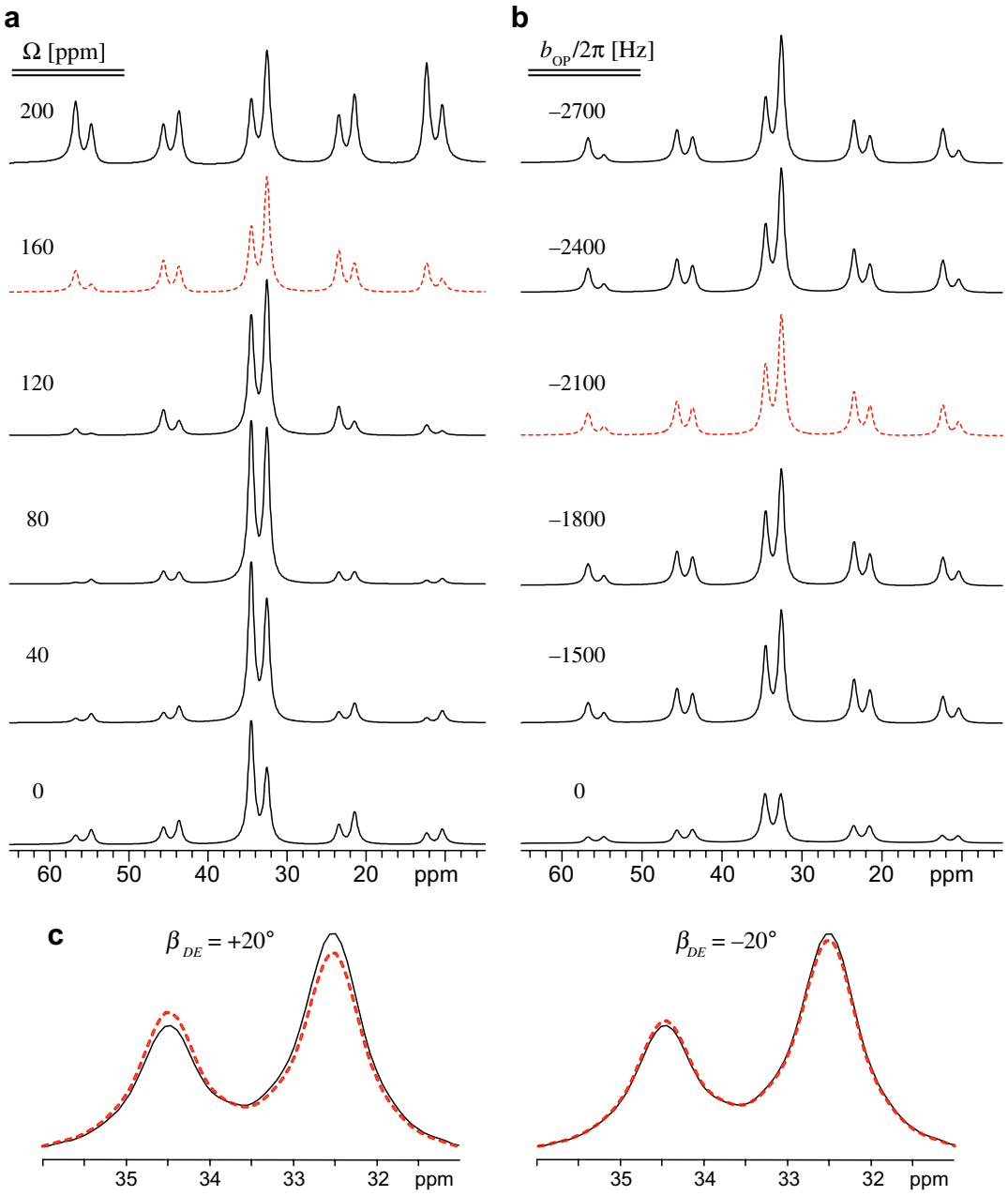

Fig. 10. Simulated ^{17}O DOR NMR spectra (*without* ssb suppression) of $OPPh_3$ at $B_0 = 14.1$ T showing effects of varying (a) Ω, (b) $b_{OP}/2\pi$, the ^{17}O–^{31}P dipolar interaction, and (c) the Euler angle β_{DE} between the dipole vector and the principal axis of the EFG with all other parameters held to the best fit values given in Table 1. Best-fit simulations shown as dashed lines.

less sensitive to the magnitude of the dipolar interaction (Fig. 10b), although they do exhibit significant sensitivity to the Euler angle (β_{DE}) between the ^{17}O–^{31}P internuclear vector and the principal axis (V_{33}) of the EFG tensor at the ^{17}O nucleus. For the centreband it can be seen that the simulation at $\beta_{DE} = +20°$ is significantly further from the best fit ($\beta_{DE} = -5°$, shown dashed) than when $\beta_{DE} = -20°$ (Fig. 10c).

The parameters determined from these ^{17}O DOR NMR simulations (Table 1) are found to agree well with previous reported data from a combination of MAS and static spectra [56], but with much higher accuracy in the value of $^{1}J_{OP}$ (note that the Euler angles are defined differently in [56]). Note that, as was the case for L-alanine, the observed spectrum is also sensitive to κ and the angles relating the CS and EFG PASs. For the determination of β_{DE} the value of the dipolar coupling constant was fixed at that calculated from the known O–P distance in the crystal structure [64]. The uncertainty in β_{DE} would be somewhat greater if $b_{OP}/2\pi$ were unknown, nevertheless both β_{DE} and $b_{OP}/2\pi$ could be determined solely from the DOR spectrum with approximate accuracies of ±20° for β_{DE} and ±400 Hz for $b_{OP}/2\pi$. A further advantage of DOR is that since the Euler angle β_{DE} is determined, the CSA and EFG parameters

may be directly related to the molecular frame and, since $\beta_{DE} \sim -5°$, V_{33} is close to the O–P internuclear axis as predicted in the calculation of Ref. [56]. Furthermore, given that $\beta_{CE} = 4°$, δ_{33} is also nearly coincident with the O–P internuclear vector.

7. Conclusion

This work shows that using the spinning sideband intensities observed in high-resolution DOR NMR spectra, the chemical shift anisotropy and relative orientation between EFG and CS tensors can be determined to an accuracy comparable to multi-field static and MAS studies of similar compounds. Although the spectrum can become more complex when C_Q and/or Ω is large, it should still be possible to extract these parameters. However, for best results, it is necessary to have an accurate description of the EFG parameters which can usually be provided by MAS spectra. The high resolution provided by DOR also has the advantage that more precise values of smaller couplings such as the J coupling in $OPPh_3$ can be obtained. Furthermore, for such a case where a splitting due to the heteronuclear J coupling is observed, it is possible to determine the angle between the internuclear vector and the principal axis of the EFG from the relative intensity of the split DOR peaks. Thus the orientation of the major components of both the EFG and chemical shift tensors in the molecular frame may be obtained. While a comparison with MQMAS is beyond the scope of this article, it has been shown that the spinning sideband patterns in isotropic MQMAS spectra are sensitive to the chemical shift tensor parameters [65] and its relative orientation to the EFG tensor [66,67].

It is envisioned that DOR can be of particular value for systems with multiple quadrupolar sites, which would be difficult to characterize otherwise (even with MQMAS). Take for example, monosodium glutamate, which has 8 oxygen sites, whose ^{17}O MAS NMR spectrum is almost featureless [38,41]. The much higher sensitivity achieved by utilizing DOR, not only attains high-resolution spectra without requiring lengthy 2D acquisitions, but also opens up the possibility of fully characterizing each site by using the simulation program described herein. Another potential application arises when CSA is relatively small, as simulations have shown that the DOR ssb intensities are still affected for spans of $\geqslant 20$ ppm unless the second-order quadrupole broadening is very much larger than the CSA.

Acknowledgments

Funding from EPSRC, BBSRC and the University of Warwick is acknowledged. I.H. and R.D. thank the Leverhulme Trust for funding. S.P.B. thanks the EPSRC for the award of an ARF. A.W. thanks the NSERC of Canada for a Post-Doctoral Fellowship Award.

References

[1] M.E. Smith, E.R.H. van Eck, Prog. Nucl. Magn. Reson. Spectrosc. 34 (1999) 159.
[2] A. Llor, J. Virlet, Chem. Phys. Lett. 152 (1988) 248.
[3] A. Samoson, E. Lippmaa, A. Pines, Mol. Phys. 65 (1988) 1013.
[4] K.T. Mueller, B.Q. Sun, G.C. Chingas, J.W. Zwanziger, T. Terao, A. Pines, J. Magn. Reson. 86 (1990) 470.
[5] L. Frydman, J.S. Harwood, J. Am. Chem. Soc. 117 (1995) 5367.
[6] A. Medek, J.S. Harwood, L. Frydman, J. Am. Chem. Soc. 117 (1995) 12779.
[7] S.P. Brown, S. Wimperis, J. Magn. Reson. 128 (1997) 42.
[8] Z.H. Gan, J. Am. Chem. Soc. 122 (2000) 3242.
[9] S.E. Ashbrook, S. Wimperis, Prog. Nucl. Magn. Reson. Spectrosc. 45 (2004) 53.
[10] M.J. Thrippleton, T.J. Ball, S. Steuernagel, S.E. Ashbrook, S. Wimperis, Chem. Phys. Lett. 431 (2006) 390.
[11] A. Samoson, E. Lippmaa, J. Magn. Reson. 84 (1989) 410.
[12] A. Samoson, Chem. Phys. Lett. 214 (1993) 456.
[13] A. Samoson, J. Tegenfeldt, J. Magn. Reson. Ser. A 110 (1994) 238.
[14] D. Kuwahara, T. Nakai, Chem. Phys. Lett. 260 (1996) 249.
[15] A. Samoson, T. Anupold, Solid State Nucl. Magn. Reson. 15 (2000) 217.
[16] A.P.M. Kentgens, E.R.H. van Eck, T.G. Ajithkumar, T. Anupold, J. Past, A. Reinhold, A. Samoson, J. Magn. Reson. 178 (2006) 212.
[17] A.P. Howes, T. Anupold, V. Lemaitre, A. Kukol, A. Watts, A. Samoson, M.E. Smith, R. Dupree, Chem. Phys. Lett. 421 (2006) 42.
[18] B.F. Chmelka, K.T. Mueller, A. Pines, J. Stebbins, Y. Wu, J.W. Zwanziger, Nature 339 (1989) 42.
[19] K.T. Mueller, Y. Wu, B.F. Chmelka, J. Stebbins, A. Pines, J. Am. Chem. Soc. 113 (1991) 32.
[20] Z. Xu, B.L. Sherriff, Appl. Magn. Reson. 4 (1993) 203.
[21] D. Massiot, D. Muller, T. Hubert, M. Schneider, A.P.M. Kentgens, B. Cote, J.P. Coutures, W. Gessner, Solid State Nucl. Magn. Reson. 5 (1995) 175.
[22] R.E. Youngman, S.T. Haubrich, J.W. Zwanziger, M.T. Janicke, B.F. Chmelka, Science 269 (1995) 1416.
[23] K.J.D. MacKenzie, M.E. Smith, M. Schmucker, H. Schneider, P. Angerer, Z. Gan, T. Anupold, A. Reinhold, A. Samoson, Phys. Chem. Chem. Phys. 3 (2001) 2137.
[24] D. Prochnow, A.R. Grimmer, D. Freude, Solid State Nucl. Magn. Reson. 30 (2006) 69.
[25] I. Hung, A.P. Howes, T. Anupold, A. Samoson, D. Massiot, M.E. Smith, S.P. Brown, R. Dupree, Chem. Phys. Lett. 432 (2006) 152.
[26] C. Rohrig, I. Dierdorf, H. Gies, J. Phys. Chem. Solids 56 (1995) 1369.
[27] R. Jelinek, A. Malek, G.A. Ozin, J. Phys. Chem. 99 (1995) 9236.
[28] L.M. Bull, B. Bussemer, T. Anupold, A. Reinhold, A. Samoson, J. Sauer, A.K. Cheetham, R. Dupree, J. Am. Chem. Soc. 122 (2000) 4948.
[29] J.E. Readman, C.P. Grey, M. Ziliox, L.M. Bull, A. Samoson, Solid State Nucl. Magn. Reson. 26 (2004) 153.
[30] A. Stein, G.A. Ozin, G.D. Stucky, J. Am. Chem. Soc. 114 (1992) 8119.
[31] G. Engelhardt, P. Sieger, J. Felsche, Anal. Chim. Acta 283 (1993) 967.
[32] G. Engelhardt, H. Koller, P. Sieger, W. Depmeier, A. Samoson, Solid State Nucl. Magn. Reson. 1 (1992) 127.
[33] M.P.J. Peeters, J.W. Dehaan, L.J.M. Vandeven, J.H.C. Vanhooff, J. Phys. Chem. 97 (1993) 5363.
[34] J. Janchen, M.P.J. Peeters, J.W. Dehaan, L.J.M. Vandeven, J.H.C. Vanhooff, I. Girnus, U. Lohse, J. Phys. Chem. 97 (1993) 12042.
[35] Y. Wu, D. Lewis, J.S. Frye, A.R. Palmer, R.A. Wind, J. Magn. Reson. 100 (1992) 425.
[36] Y. Wu, B.F. Chmelka, A. Pines, M.E. Davis, P.J. Grobet, P.A. Jacobs, Nature 346 (1990) 550.
[37] A. Samoson, P. Sarv, J.P.V. Houckgeest, B. Kraushaarczarnetzki, Appl. Magn. Reson. 4 (1993) 171.
[38] V. Lemaitre, K.J. Pike, A. Watts, T. Anupold, A. Samoson, M.E. Smith, R. Dupree, Chem. Phys. Lett. 37 (2003) 91.

[39] K.J. Pike, V. Lemaitre, A. Kukol, T. Anupold, A. Samoson, A.P. Howes, A. Watts, M.E. Smith, R. Dupree, J. Phys. Chem. B 108 (2004) 9256.
[40] A. Wong, K.J. Pike, R. Jenkins, G.J. Clarkson, T. Anupold, A.P. Howes, D.H.G. Crout, A. Samoson, R. Dupree, M.E. Smith, J. Phys. Chem. A 110 (2006) 1824.
[41] A. Wong, A.P. Howes, K.J. Pike, V. Lemaitre, A. Watts, T. Anupold, J. Past, A. Samoson, R. Dupree, M.E. Smith, J. Am. Chem. Soc. 128 (2006) 7744.
[42] J.P. Amoureux, E. Cochon, Solid State Nucl. Magn. Reson. 2 (1993) 223.
[43] S.E. Ashbrook, M.E. Smith, Chem. Soc. Rev. 35 (2006) 718.
[44] V. Lemaitre, M.E. Smith, A. Watts, Solid State Nucl. Magn. Reson. 26 (2004) 215.
[45] M. Bak, J.T. Rasmussen, N.C. Nielsen, J. Magn. Reson. 147 (2000) 296.
[46] M. Eden, Concept Magn. Reson. A 18A (2003) 1.
[47] M. Eden, Concept Magn. Reson. A 18A (2003) 24.
[48] M. Eden, Concept Magn. Reson. A 17A (2003) 117.
[49] P. Hodgkinson, L. Emsley, Prog. Nucl. Magn. Reson. Spectrosc. 36 (2000) 201.
[50] B.Q. Sun, J.H. Baltisberger, Y. Wu, A. Samoson, A. Pines, Solid State Nucl. Magn. Reson. 1 (1992) 267.
[51] E. Cochon, J.P. Amoureux, Solid State Nucl. Magn. Reson. 2 (1993) 205.
[52] R.N. Zare, Angular Momentum: Understanding Spatial Aspects in Chemistry and Physics, John Wiley and Sons, New York, 1988.
[53] M. Hohwy, H. Bildsoe, H.J. Jakobsen, N.C. Nielsen, J. Magn. Reson. 136 (1999) 6.
[54] M.H. Levitt, J. Magn. Reson. 82 (1989) 427.
[55] J. Mason, Solid State Nucl. Magn. Reson. 2 (1993) 285.
[56] D.L. Bryce, K. Eichele, R.E. Wasylishen, Inorg. Chem. 42 (2003) 5085.
[57] R.D. Sammons, P.A. Frey, K. Bruzik, M.D. Tsai, J. Am. Chem. Soc. 105 (1983) 5455.
[58] S.A. Smith, T.O. Levante, B.H. Meier, R.R. Ernst, J. Magn. Reson. Ser. A 106 (1994) 75.
[59] C. Gervais, R. Dupree, K.J. Pike, C. Bonhomme, M. Profeta, C.J. Pickard, F. Mauri, J. Phys. Chem. A 109 (2005) 6960.
[60] J.F. Baugher, P.C. Taylor, T. Oja, P.J. Bray, J. Chem. Phys. 50 (1969) 4914.
[61] J.T. Cheng, J.C. Edwards, P.D. Ellis, J. Phys. Chem. 94 (1990) 553.
[62] K. Yamada, M. Asanuma, H. Honda, T. Nemoto, T. Yamazaki, H. Hirota, J. Mol. Struct. in press, doi:10.1016/j.molstruc.2006.12.034.
[63] J.R. Yates, 2007, private communication.
[64] C.P. Brock, W.B. Schweizer, J.D. Dunitz, J. Am. Chem. Soc. 107 (1985) 6964.
[65] S.H. Wang, Z. Xu, J.H. Baltisberger, L.M. Bull, J.F. Stebbins, A. Pines, Solid State Nucl. Magn. Reson. 8 (1997) 1.
[66] T. Charpeutier, J. Virlet, Solid State Nucl. Magn. Reson. 12 (1998) 227.
[67] A. Lupulescu, S.P. Brown, H.W. Spiess, J. Magn. Reson. 154 (2002) 101.